STRUCTURAL CHEMISTRY

ISSN: 2053-2296
journals.iucr.org/c

Effect of the ammonium ion on proton conduction in porous ionic crystals based on Keggin-type silicododecatungstate

Satoru Miyazawa, Reina Hosono, Ryota Osuga, Junko Nomura Kondo and Sayaka Uchida

Acta Cryst. (2018). C**74**, 1289–1294

STRUCTURAL CHEMISTRY
ISSN 2053-2296

Effect of the ammonium ion on proton conduction in porous ionic crystals based on Keggin-type silicododecatungstate

Satoru Miyazawa,[a] Reina Hosono,[a] Ryota Osuga,[b] Junko Nomura Kondo[b] and Sayaka Uchida[a]*

[a]Department of Basic Science, School of Arts and Sciences, The University of Tokyo, 3-8-1 Komaba, Meguroku, Tokyo 153-8902, Japan, and [b]Laboratory for Chemistry and Life Science, Institute of Innovative Research, Tokyo Institute of Technology, 4259-R1-10 Nagatsuta, Midori-ku, Yokohama, Kanagawa 226-8503, Japan. *Correspondence e-mail: csayaka@mail.ecc.u-tokyo.ac.jp

Received 13 April 2018
Accepted 4 June 2018

Edited by J. R. Galán-Mascarós, Institute of Chemical Research of Catalonia (ICIQ), Spain

Keywords: proton conduction; silicododecatungstate; polyoxometalate; ammonium ion; porous crystal; crystal structure.

CCDC reference: 1835687

Supporting information: this article has supporting information at journals.iucr.org/c

Proton conduction in crystalline porous materials has received much attention from basic scientific research through to practical applications. Polyoxometalates (POMs) can efficiently transport protons because of their small superficial negative charge density. A simple method for enhancing proton conductivity is to introduce NH_4^+ into the crystal structure, because NH_4^+ can form hydrogen bonds and function as a proton carrier. According to these considerations, NH_4^+ was introduced into the porous structure of $A_2[Cr_3O(OOCH)_6(etpy)_3]_2[\alpha\text{-}SiW_{12}O_{40}]\cdot nH_2O$ (A = Li, Na, K and Cs; etpy = 4-ethylpyridine) (**I-A$^+$**) *via* topotactic cation exchange. The resulting compound, diammonium tris(4-ethylpyridine)hexaformatooxidotrichromium α-silicododecatungstate hexahydrate, $(NH_4)_2[Cr_3(CHO_2)_6O(C_7H_9N)_3]_2[\alpha\text{-}SiW_{12}O_{40}]\cdot 6H_2O$, showed high proton conductivity and low activation energy under high relative humidity (RH), suggesting that protons migrate efficiently *via* rearrangement of the hydrogen-bonding network formed by the NH_4^+ cations and the waters of crystallization (Grotthuss mechanism). The proton conductivity and activation energy greatly decreased and increased, respectively, with the decrease in RH, suggesting that protons migrate as NH_4^+ and/or H_3O^+ under low RH (vehicle mechanism).

1. Introduction

Proton-conducting solid electrolytes have been studied extensively from points of view ranging from basic research to practical applications (Norby, 1999). In particular, proton conduction in crystalline porous materials, such as metal–organic frameworks (MOFs) and zeolites, have attracted much interest because the rational design and chemical tuning of the porous framework allow chemists to control the functional properties (see, for example, Kreuer *et al.*, 1982; Horike *et al.*, 2013). Polyoxometalates (POMs), which are nano-sized anionic metal–oxygen clusters of early transition metals (see, for example, Long *et al.*, 2007; Proust *et al.*, 2008; Kortz *et al.*, 2009), can efficiently transport protons since smearing of the negative charge over the external surface O atoms makes the effective surface charge density small. In fact, acid salts of Keggin-type POMs ($H_3PW_{12}O_{40}$ and $H_4SiW_{12}O_{40}$) exhibit high proton conductivities comparable to commercial Nafion membranes under high relative humidity (RH) (Nakamura *et al.*, 1981). However, application of POM-based compounds has been limited by the lack of structural stability and a large decrease of conductivity with respect to a slight decrease in RH.

We have been working on proton conduction in ionic crystals based on POMs (Tsuboi *et al.*, 2016; Niinomi *et al.*,

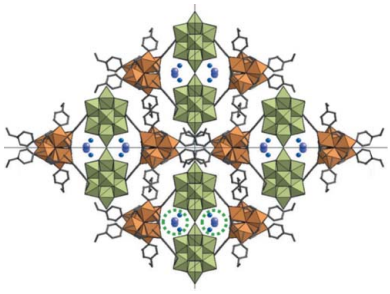

2017; Uchida *et al.*, 2017). In one of our previous works, a series of alkali metal ion-exchanged porous ionic crystals based on Keggin-type silicododecatungstate, *viz.* $A_2[Cr_3O(OOCH)_6(etpy)_3]_2[\alpha\text{-}SiW_{12}O_{40}]\cdot nH_2O$ (A = Li, Na, K and Cs; etpy = 4-ethylpyridine) (**I-A$^+$**) were synthesized and it was demonstrated that **I-A$^+$** with alkali metal ions of high ionic potentials (z/r, where r is the ionic radius and z is the charge) form dense and extensive hydrogen-bonding networks of water molecules, which leads to high proton conductivities and low activation energies (Uchida *et al.*, 2017).

A simple method for enhancing proton conductivity is to introduce NH_4^+ into the porous structure; NH_4^+ can form hydrogen bonds and function as a proton carrier (pK_a of NH_4^+ is 9.25; Pliego *et al.*, 2002). There have been several reports on proton conduction in crystalline porous materials containing NH_4^+. For example, a MOF of $(NH_4)_2(H_2adp)[Zn(ox)_3]\cdot 3H_2O$ (H_2adp = adipic acid and ox = oxalate) showed a proton conductivity of $>10^{-4}$ S cm^{-1} at room temperature (rt), and the value decreased significantly to 10^{-6} S cm^{-1} by topotactic cation exchange of NH_4^+ with K^+ (Sadakiyo *et al.*, 2009, 2014). The layered zirconium phosphate $(NH_4)_2[ZrF_2(HPO_4)_2]$ showed an extremely high proton conductivity of $>10^{-2}$ S cm^{-1} at 363 K and RH95% (relative humidity), with a small activation energy of 0.19 eV (Gui *et al.*, 2016). This compound can conduct protons in the intermediate temperature range (383–503 K) without humidification, and the activation energy increased to 0.46 eV. It was concluded that, under low temperatures and high RH, a dense hydrogen-bonding network of H_2O and NH_4^+ is formed, which enables efficient proton transport (Grotthuss mechanism; see, Kreuer, 1996), while under intermediate temperatures without humidification, NH_4^+ is thermally activated as a proton carrier (vehicle mechanism; see, Kreuer, 1996). It was recently revealed by diffuse reflection Fourier transform IR spectroscopy measurements that in the catalytic reduction of NOx with NH_3 (*i.e.* NH_3- SCR) by zeolites, NH_3 serves as a vehicle in the proton-transfer reaction and that proton-conducting NH_4^+ intermediates are the key to high catalytic activity (Chen *et al.*, 2016).

According to these observations, we introduced NH_4^+ into the porous structure of **I-A$^+$** *via* topotactic cation exchange and investigated the proton conductivity (303–363 K). Compound **I-NH$_4^+$** showed high proton conductivity under high RH (2.5×10^{-3} S cm^{-1} at 363 K and RH95%), which can be classified as a highly proton-conductive solid, and the activation energy was small (0.22 eV), suggesting that protons mostly migrate *via* rearrangement of the hydrogen-bonding network (Grotthuss mechanism). The proton conductivity decreased greatly with the decrease in RH (10^{-8}–10^{-7} S cm^{-1} at RH50%) and the activation energy increased up to 0.88 eV, suggesting that protons migrate as NH_4^+ and/or H_3O^+ under low RH (vehicle mechanism).

Table 1
Experimental details.

Crystal data	
Chemical formula	$(NH_4)_2[Cr_3(CHO_2)_6O(C_7H_9N)_3]_2[SiW_{12}O_{40}]\cdot 6H_2O$
M_r	4491.50
Crystal system, space group	Monoclinic, $C2/c$
Temperature (K)	93
a, b, c (Å)	32.303 (4), 25.546 (3), 13.561 (2)
β (°)	110.885 (6)
V (Å^3)	10456 (2)
Z	4
Radiation type	Mo $K\alpha$
μ (mm^{-1})	13.87
Crystal size (mm)	0.20 × 0.20 × 0.20
Data collection	
Diffractometer	Rigaku Saturn70
Absorption correction	Multi-scan (*REQAB*; Rigaku, 1998)
T_{min}, T_{max}	0.009, 0.062
No. of measured, independent and observed [$F^2 > 2.0\sigma(F^2)$] reflections	35536, 9475, 7855
R_{int}	0.056
(sin $\theta/\lambda)_{max}$ (Å^{-1})	0.602
Refinement	
$R[F^2 > 2\sigma(F^2)]$, $wR(F^2)$, S	0.058, 0.175, 1.11
No. of reflections	9475
No. of parameters	662
H-atom treatment	H-atom parameters not defined
$\Delta\rho_{max}$, $\Delta\rho_{min}$ (e Å^{-3})	3.11, −3.90

Computer programs: *CrystalClear* (Rigaku, 2007), *SHELXL97* (Sheldrick, 2008), *SHELXL2014* (Sheldrick, 2015) and *CrystalStructure* (Rigaku, 2015).

2. Experimental

2.1. Synthesis

$K_2[Cr_3O(OOCH)_6(etpy)_3]_2[\alpha\text{-}SiW_{12}O_{40}]\cdot 8H_2O$ (etpy = 4-ethylpyridine), **I-K$^+$**, was synthesized according to our previous work (Eguchi *et al.*, 2012). Cation exchange was carried out by immersing **I-K$^+$** (0.1 g, 2.2×10^{-2} mmol) in 25 ml of 0.3 mol l^{-1} NH_4NO_3 (aq) (NH_4^+: 7.5 mmol), followed by stirring at room temperature (rt) for 24 h. The compound was collected by suction filtration, followed by washing with water and drying under reduced pressure (yield 90%). The chemical formula of the resulting compound was determined as $(NH_4)_2[Cr_3O(OOCH)_6(etpy)_3]_2[\alpha\text{-}SiW_{12}O_{40}]\cdot 6H_2O$ (**I-NH$_4^+$**) [elemental analysis for $C_{54}H_{86}Cr_6N_8O_{72}SiW_{12}$ (calculated) (%): C 14.27 (14.27), H 1.70 (1.91), N 2.26 (2.47), Cr 7.11 (6.86), K 0.0 (0.0), Si 0.62 (0.62), W 50.96 (48.53)] *via* CHN combustion analysis, inductively coupled plasma optical emission spectrometry (ICP-OES) and thermogravimetry (TG; Fig. S1 in the supporting information). It was shown by atomic absorption spectrometry (AAS) that **I-NH$_4^+$** did not contain K and that the cation-exchange reaction was carried out to completion.

2.2. Characterization

Combustion analysis (Elementar, vario MICRO cube) was used for the quantitative analysis of C, H and N. ICP-OES (Agilent Technologies, ICP-OES720) was used for the quantitative analysis of P and W. AAS (Hitachi, ZA3000) was used for the quantitative analysis of K in **I-A$^+$**. Powder X-ray diffraction (PXRD) patterns were measured with a D8 Advance X-ray diffractometer (Bruker) using Cu $K\alpha$ radia-

tion (λ = 1.54056 Å, 40 kV–40 mA) at 2θ = 3–40° and 1.8° min^{-1}. Alternating current (AC) impedance measurements: about 0.2 g of the compounds were compressed at 150 kgf cm^{-2} into pellets of 10 mm in diameter and *ca* 1.0 mm in thickness. For the measurements at high RH, the pellets were cut into quarters and one of these quarters was used for the AC impedance measurement. The measurements were carried out in a heat chamber at 303–363 K with a BioLogic VMP3 multi-channel Potentiostat/Galvanostat (Science Instruments) over the frequency range from 2 Hz to 2 MHz and with AC amplitudes of 500 mV. Gold electrodes with copper wire were attached to both faces of the pellets. Bulk conductivities were estimated by semicircle fitting of Nyquist plots (see supporting information for details). Water vapour sorption isotherms were measured at 303 K using a Belsorp-max volumetric adsorption apparatus (BEL Japan). Prior to the measurement, about 0.1 g of crystals were ground and treated *in vacuo* at 373 K for 3 h to remove the water of crystallization. Sorption equilibrium was judged by the following criteria: ±0.3% of pressure change in 500 s. *In situ* IR spectra under water vapour were measured as follows: each powder sample was deposited on a CaF_2 plate (20 mm diameter), which was placed inclined at the centre of an IR cell, and treated *in vacuo* at 373 K for 2 h. IR spectra were obtained at a resolution of 4 cm^{-1} using a JASCO 6100 FT–IR spectrometer equipped with an MCT detector. The IR spectra of the sample in a vacuum were recorded as background spectra. The IR spectra of the adsorbed water were measured by increasing the water vapour pressure from 5 to 1 × 10^3 Pa at rt; background-subtracted IR spectra showing adsorbed water are presented throughout this article.

2.3. Single-crystal X-ray diffraction (SXRD) analysis

Single crystals of **I-NH$_4^+$** were prepared by immersing single crystals of **I-K$^+$** in 0.3 mol l^{-1} NH_4NO_3 (aq) for three weeks. Crystal data, data collection and structure refinement details are summarized in Table 1. All atoms were refined anisotropically, except that the N atoms of NH_4^+, the O atoms of the waters of crystallization and the Si atom and disordered O atoms in the [SiO_4] unit of the POM were refined isotropically. H atoms were not included in the model. The N and O atoms of NH_4^+ and water of crystallization, respectively, were distinguished according to the positions of the A^+ cation in the crystal structures of **I-A$^+$** (Uchida *et al.*, 2017) and the differences in electron densities (the N and O atoms possess site occupancies of 1.0 and 0.5, respectively).

3. Results and discussion

Compound **I-NH$_4^+$** was synthesized *via* cation-exchange reaction by immersing **I-K$^+$** (0.1 g, 2.2 × 10^{-2} mmol) in 25 ml of 0.3 mol l^{-1} NH_4NO_3 (aq) (7.5 mmol of NH_4^+), followed by stirring at room temperature (rt) for 24 h. AAS showed that **I-NH$_4^+$** did not contain K and that the cation-exchange reaction was carried out completely. The chemical formula of **I-NH$_4^+$** was determined as $(NH_4)_2[Cr_3O(OOCH)_6(etpy)_3]_2[\alpha$-$SiW_{12}O_{40}]\cdot 6H_2O$ by CHN combustion analysis, ICP-OES and TG (Fig. S1 in the supporting information). The IR spectrum (Fig. S2 in the supporting information) and the PXRD pattern (Fig. 1) of **I-NH$_4^+$** were analogous to those of **I-A$^+$**, showing that the cation-exchange treatment had little effect on the molecular and crystal structures.

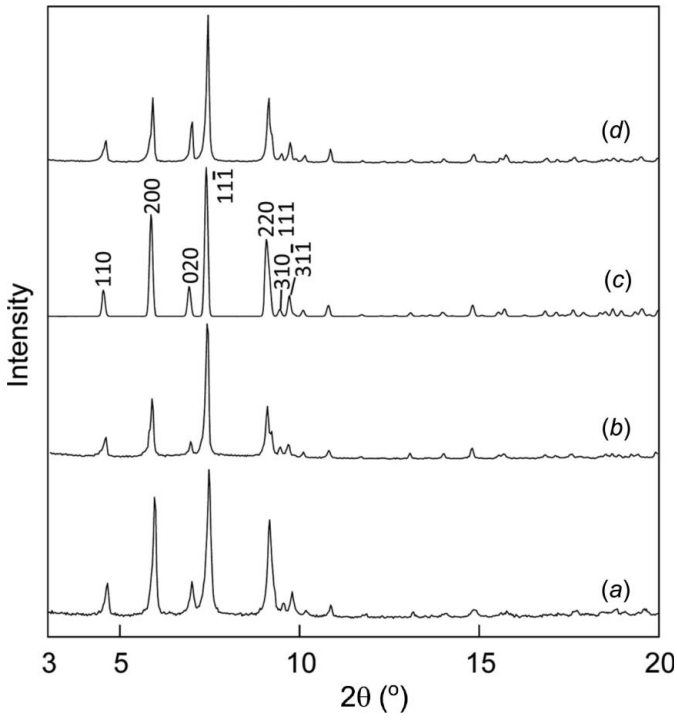

Figure 1
PXRD patterns of (*a*) **I-Li$^+$**, (*b*) **I-K$^+$**, (*c*) **I-NH$_4^+$** (calculated) and (*d*) **I-NH$_4^+$** (experimental). The numbers in part (*c*) indicate the Miller indices.

SXRD analysis of **I-NH$_4^+$** showed that one-dimensional channels with a minimum aperture of 3.5 Å, which are analogous to those of **I-A$^+$** (Uchida *et al.*, 2017), existed along the *c* axis (Fig. 2). The structure of **I-NH$_4^+$** was stabilized by π–π interactions (*ca* 3.7 Å) between the etpy ligands of neighbouring molecular cations, *i.e.* $[Cr_3O(OOCH)_6(etpy)_3]^+$. Two NH_4^+ cations per formula (2 mol mol^{-1}) were located on crystallographically equivalent sites. The Keggin ion lies on a crystallographic twofold symmetry axis. NH_4^+ existed in the one-dimensional channel and in the vicinity of the formate O atom of the molecular cation [O···N = 3.08 (3) Å] and the POM [O···N = 3.28 (4) Å]. Three of the six molecules of water of crystallization could be located with SXRD. These were located in the one-dimensional channel and existed in the vicinity of the POM, with O···O distances of 2.96 (4)–3.14 (4) Å. As shown in Fig. 2(*c*), the NH_4^+ cations and the water molecules were in hydrogen-bonding distances with respect to each other [N···O*W* = 2.62 (5) Å and O*W*···O*W* = 2.76 (4)–3.24 (5) Å, where O*W* is the O atom of a water of crystallization]. The distances were shorter than those in **I-Cs$^+$** [Cs···O*W* = 2.91 (2)–3.45 (4) Å and O*W*···O*W* = 2.92 (3)—3.14 (4) Å; Uchida *et al.*, 2017], suggesting that the dense hydrogen-bonding network in **I-NH$_4^+$** would contribute to efficient proton conduction (see below).

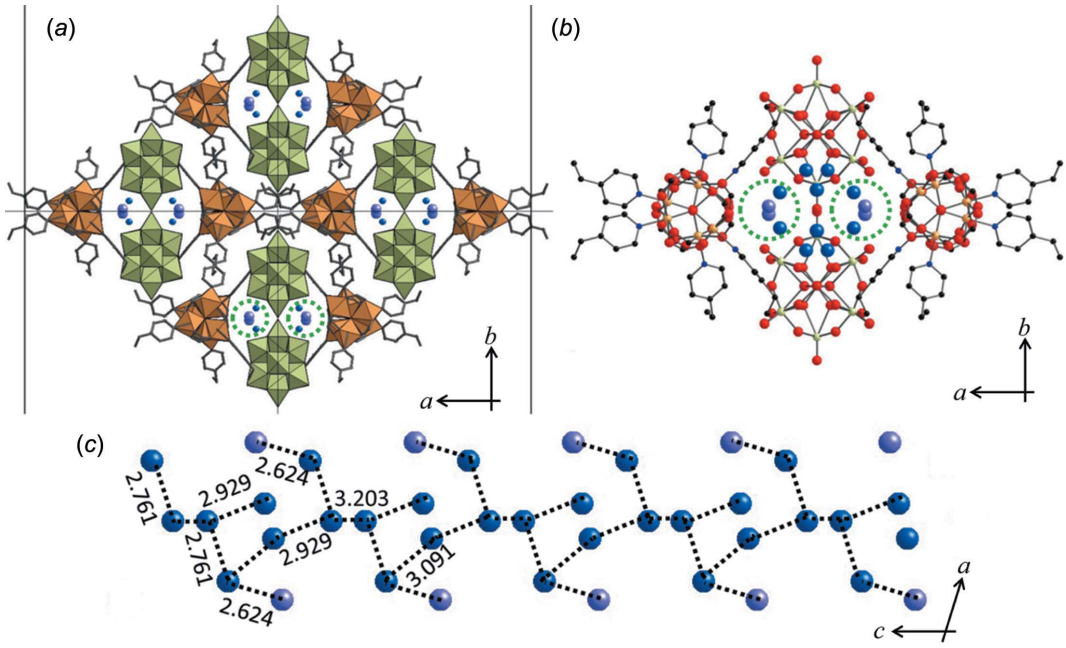

Figure 2
The crystal structure of **I-NH$_4^+$**, shown with (*a*) a polyhedral and (*b*) a ball-and-stick representation. (*c*) The positions of the N atoms of the NH_4^+ cations and the O atoms of the waters of crystallization along the one-dimensional channel (*c* axis). Green broken circles in parts (*a*) and (*b*) indicate the one-dimensional channels. The black broken lines in part (*c*) indicate the possible hydrogen bonds. The numbers represent distances (Å). Green and orange polyhedra in part (*a*) show the [WO_6] and [CrO_5N] units, respectively. Purple and blue spheres show the N atoms of the NH_4^+ cations and the O atoms of waters of crystallization, respectively. Red, orange and black spheres in part (*b*) show the O, Cr and C atoms, respectively.

Nyquist plots of the impedance spectra of a pelleted sample of **I-NH$_4^+$** were measured at 303–363 K and RH95% (Fig. S3 in the supporting information). Proton conductivities were estimated by the semicircle fitting of Nyquist plots. The proton conductivities of **I-NH$_4^+$** were 6.0×10^{-4} and 2.5×10^{-3} S cm^{-1} at 303 and 363 K, respectively, and **I-NH$_4^+$** can be classified as a highly proton-conductive solid. The activation energy estimated from the Arrhenius plot (T^{-1} *versus* logσ) of the temperature-dependent proton conductivities was 0.22 eV (Fig. 3*a*), which is small. Therefore, proton conduction in **I-NH$_4^+$** at RH95% is probably due to the Grotthuss mechanism, where protons mostly migrate *via* the extensive hydrogen-bonding network formed by NH_4^+ and H_2O (see Fig. 2*c*).

In our previous work, **I-Li$^+$** showed the highest proton conductivity (> 10^{-3} S cm^{-1}) among **I-A$^+$** at 303–323 K and RH95%, and the activation energy decreased in the order of **I-Cs$^+$** (0.75 eV) > **I-K$^+$** (0.56 eV) > **I-Na$^+$** (0.33 eV) > **I-Li$^+$** (0.23 eV) (Uchida *et al.*, 2017). In order to compare the results of **I-NH$_4^+$** with those of **I-Li$^+$**, additional measurements were carried out for **I-Li$^+$** and the activation energy was re-estimated in the range 303–363 K. The proton conductivity and activation energy of **I-Li$^+$** were 8.4×10^{-3} S cm^{-1} (363 K) and 0.29 eV (Fig. S4 in the supporting information), respectively. Both proton conductivities and activation energies were in the order **I-Li$^+$** > **I-NH$_4^+$**, which can be interpreted as follows. As

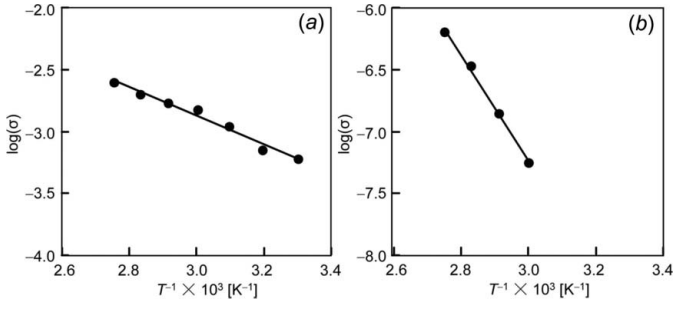

Figure 3
Arrhenius plots of the temperature-dependent proton conductivities of **I-NH$_4^+$** at relative humidities (RH) of (*a*) 95% (303–363 K) and (*b*) 50% (333–363 K).

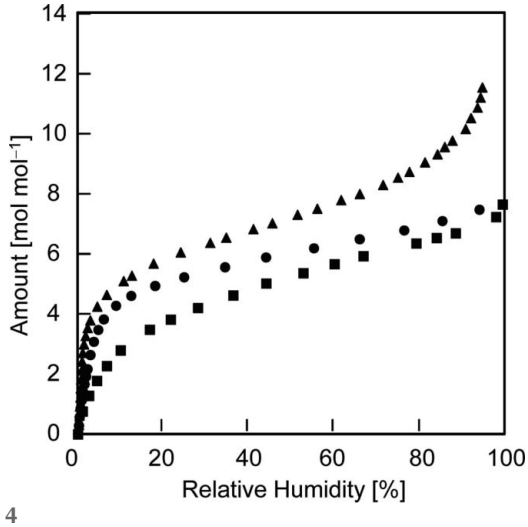

Figure 4
Water-sorption isotherms of **I-A$^+$** at 303 K. Triangles, circles and squares show the data for **I-Li$^+$**, **I-K$^+$** and **I-NH$_4^+$**, respectively.

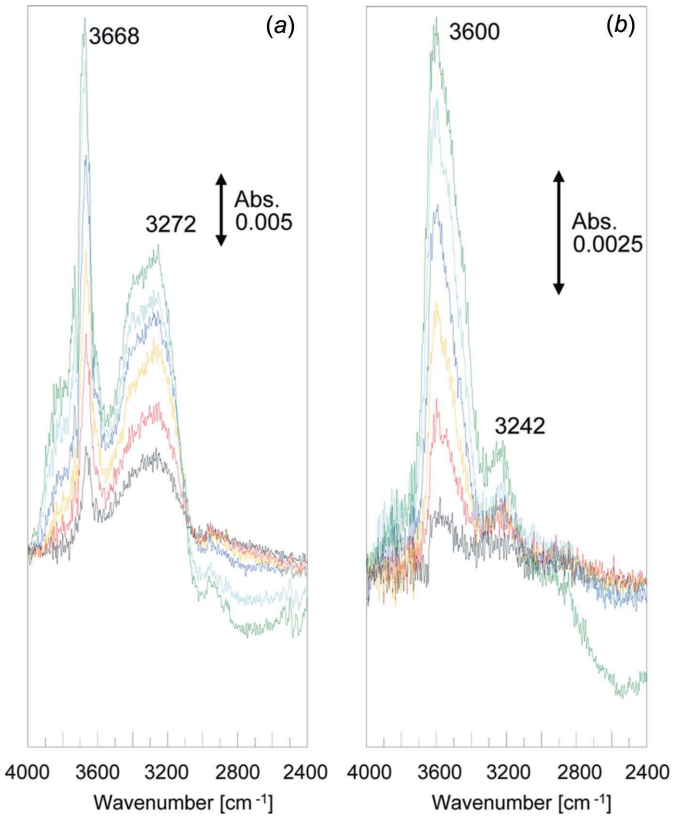

Figure 5
Changes in the IR spectra (298 K) of (*a*) **I-Li$^+$** and (*b*) **I-NH$_4^+$** under a water vapour pressure between 5 and 1 × 10^3 Pa.

shown by the water-sorption isotherms (Fig. 4), the amounts of water sorption were in the order **I-Li$^+$** > **I-K$^+$** > **I-NH$_4^+$** throughout the whole RH range. This is in line with the order of ionic potentials of the cations (z/r: $Li^+ > K^+ > NH_4^+$; r is from Shannon, 1976; Sidey, 2016), and thus with the order of the ion–dipole interactions between the cations and water molecules. Therefore, the numbers of proton carriers (or proton density) should be in the order **I-Li$^+$** > **I-NH$_4^+$**, which is in line with the higher proton conductivity of **I-Li$^+$**. Considering the proton transfer along the hydrogen-bonding network in the one-dimensional channels, while NH_4^+ can donate protons, participate in hydrogen bonding and transfer protons, Li^+ cannot, which is probably responsible for the lower activation energy of **I-NH$_4^+$** with repsect to **I-Li$^+$**.

Next, Nyquist plots of the impedance spectra of a pelleted sample of **I-NH$_4^+$** were measured under low RH (Fig. S5 in the supporting information). Proton conductivity decreased significantly by 3–4 orders of magnitude (10^{-8}–10^{-7} S cm^{-1}) with the decrease in RH from 95 to 50%. The activation energy estimated from the Arrhenius plot (T^{-1} *versus* logσ) of the temperature-dependent proton conductivities was 0.88 eV (Fig. 3*b*), which is quite large, suggesting that protons migrate as NH_4^+ and/or H_3O^+ at low RH (vehicle mechanism).

Finally, the states of water in **I-NH$_4^+$** was investigated with the ν(OH) bands of the *in situ* IR spectra. The spectra of **I-NH$_4^+$** and **I-Li+**, as a reference, are shown in Fig. 5. Upon the introduction of water vapour, two bands appeared at above 3600 cm^{-1} and below 3300 cm^{-1}, and the intensities of these bands increased with the increase in water vapour pressure. Notably, the intensity of the band at higher frequency increased greatly for **I-NH$_4^+$** (Fig. 5*b*). In our previous work on **I-A$^+$**, the bands at higher and lower wavenumbers were attributed to the free O—H bond of water molecules at the outside of a water cluster and to the hydrogen-bonded O—H bond of water molecules inside the cluster, respectively (Jentys *et al.*, 1989; Uchida *et al.*, 2017). In addition, *ab initio* simulation studies on solvated NH_4^+ showed that the hydrogen bonds between NH_4^+ and water are strong enough to prevent the free rotation of NH_4^+, which instead tumbles in a sequence of discontinuous rotational jumps with the exchange of two water molecules (Brugé *et al.*, 1999). According to these observations, the relationship between proton conductivity and states of water molecules can be explained as follows: since the activation energy under high RH is in the order **I-NH$_4^+$** (0.22 eV) < **I-Li$^+$** (0.29 eV), and the relative intensity of the band at higher wavenumber is in the order **I-NH$_4^+$** > **I-Li$^+$**, it can be reasonably assumed that **I-NH$_4^+$** possesses more mobile protons, probably due to the existence of NH_4^+, contributing to the efficient proton transfer along the hydrogen-bonding network and thus a lower activation energy.

4. Conclusions

$(NH_4)_2[Cr_3O(OOCH)_6(etpy)_3]_2[\alpha\text{-}SiW_{12}O_{40}]\cdot 6H_2O$ (**I-NH$_4^+$**) based on Keggin-type silicododecatungstate was synthesized by topotactic cation exchange of K^+ with NH_4^+. NH_4^+ can form hydrogen bonds, function as a proton carrier and thus contribute to the enhancement of proton conductivity. As expected, **I-NH$_4^+$** exhibited high proton conductivity (> 10^{-3} S cm^{-1}) and low activation energy (0.22 eV) under high relative humidity (RH 95%). These results show that protons migrate efficiently *via* rearrangement of the hydrogen-bonding network formed by the NH_4^+ cations and the waters of crystallization. The dynamics of NH_4^+ and further utilization of NH_4^+ in POM-based compounds will be reported in due course.

Acknowledgements

Professor M. Matsuo and Dr K. Shozugawa (University of Tokyo) are acknowledged for providing access to the ICP instrument.

Funding information

Funding for this research was provided by: Grant-in-Aids for scientific research JP16K05742 and JP17H05356 (Coordination Asymmetry) from MEXT of Japan.

References

Brugé, F., Bernasconi, M. & Parrinello, M. (1999). *J. Am. Chem. Soc.* **121**, 10883–10888.
Chen, P., Moos, R. & Simon, U. (2016). *J. Phys. Chem. C*, **120**, 25361–25370.

Eguchi, R., Uchida, S. & Mizuno, N. (2012). *Angew. Chem. Int. Ed.* **51**, 1635–1639.
Gui, D., Zheng, T., Xie, J., Cai, Y., Wang, Y., Chen, L., Diwu, J., Chai, Z. & Wang, S. (2016). *Inorg. Chem.* **55**, 12508–12511.
Horike, S., Umeyama, D. & Kitagawa, S. (2013). *Acc. Chem. Res.* **46**, 2376–2384.
Jentys, A., Warecka, G., Derewinski, M. & Lercher, J. A. (1989). *J. Phys. Chem.* **93**, 4837–4843.
Kortz, U., Müller, A., van Slageren, J., Schnack, J., Dalal, N. S. & Dressel, M. (2009). *Coord. Chem. Rev.* **253**, 2315–2327.
Kreuer, K. D. (1996). *Chem. Mater.* **8**, 610–641.
Kreuer, K. D., Weppner, W. & Rabenau, A. (1982). *Mater. Res. Bull.* **17**, 501–509.
Long, D.-L., Burkholder, E. & Cronin, L. (2007). *Chem. Soc. Rev.* **36**, 105–121.
Nakamura, O., Ogino, I. & Kodama, T. (1981). *Solid State Ionics*, **3–4**, 347–351.
Niinomi, K., Miyazawa, S., Hibino, M., Mizuno, N. & Uchida, S. (2017). *Inorg. Chem.* **56**, 15187–15193.
Norby, T. (1999). *Solid State Ionics*, **125**, 1–11.
Pliego, J. R. Jr & Riveros, J. M. (2002). *Phys. Chem. Chem. Phys.* **4**, 1622–1627.
Proust, A., Thouvenot, R. & Gouzerh, P. (2008). *Chem. Commun.* pp. 1837–1852.
Rigaku (1998). *REQAB*. Rigaku Corporation, Tokyo, Japan.
Rigaku (2007). *CrystalClear*. Rigaku Corporation, Tokyo, Japan.
Rigaku (2015). *CrystalStructure*. Rigaku Corporation, Tokyo, Japan.
Sadakiyo, M., Yamada, T. & Kitagawa, H. (2009). *J. Am. Chem. Soc.* **131**, 9906–9907.
Sadakiyo, M., Yamada, T. & Kitagawa, H. (2014). *J. Am. Chem. Soc.* **136**, 13166–13169.
Shannon, R. D. (1976). *Acta Cryst.* A**32**, 751–767.
Sheldrick, G. M. (2008). *Acta Cryst.* A**64**, 112–122.
Sheldrick, G. M. (2015). *Acta Cryst.* C**71**, 3–8.
Sidey, V. (2016). *Acta Cryst.* B**72**, 626–633.
Tsuboi, M., Hibino, M., Mizuno, N. & Uchida, S. (2016). *J. Solid State Chem.* **234**, 9–14.
Uchida, S., Hosono, R., Eguchi, R., Kawahara, R., Osuga, R., Kondo, N. J., Hibino, M. & Mizuno, N. (2017). *Phys. Chem. Chem. Phys.* **19**, 29077–29083.

supporting information

Acta Cryst. (2018). C**74**, 1289-1294 [https://doi.org/10.1107/S2053229618008227]

Effect of the ammonium ion on proton conduction in porous ionic crystals based on Keggin-type silicododecatungstate

Satoru Miyazawa, Reina Hosono, Ryota Osuga, Junko Nomura Kondo and Sayaka Uchida

Computing details

Data collection: *CrystalClear* (Rigaku, 2007); cell refinement: *CrystalClear* (Rigaku, 2007); data reduction: *CrystalClear* (Rigaku, 2007); program(s) used to solve structure: *SHELXL97* (Sheldrick, 2008); program(s) used to refine structure: *SHELXL2014* (Sheldrick, 2015); molecular graphics: *CrystalStructure* (Rigaku, 2015); software used to prepare material for publication: *CrystalStructure* (Rigaku, 2015).

Diammonium tris(4-ethylpyridine)hexaformatooxidotrichromium α-silicododecatungstate

Crystal data

$(NH_4)_2[Cr_3(CHO_2)_6O(C_7H_9N)_3]_2[SiW_{12}O_{40}]\cdot 8H_2O$
$M_r = 4491.50$
Monoclinic, $C2/c$
$a = 32.303$ (4) Å
$b = 25.546$ (3) Å
$c = 13.561$ (2) Å
$\beta = 110.885$ (6)°
$V = 10456$ (2) Å^3
$Z = 4$
$F(000) = 8232.00$
$D_x = 2.853$ Mg m^{-3}
Mo $K\alpha$ radiation, $\lambda = 0.71075$ Å
Cell parameters from 15010 reflections
$\theta = 1.0$–$25.4°$
$\mu = 13.87$ mm^{-1}
$T = 93$ K
Block, brown
0.20 × 0.20 × 0.20 mm

Data collection

Rigaku Saturn70 diffractometer
Detector resolution: 7.314 pixels mm^{-1}
ω scans
Absorption correction: multi-scan (*REQAB*; Rigaku, 1998)
$T_{min} = 0.009$, $T_{max} = 0.062$
35536 measured reflections
9475 independent reflections
7855 reflections with $F^2 > 2.0\sigma(F^2)$
$R_{int} = 0.056$
$\theta_{max} = 25.3°$, $\theta_{min} = 1.0°$
$h = -38\rightarrow38$
$k = -30\rightarrow28$
$l = -14\rightarrow16$

Refinement

Refinement on F^2
$R[F^2 > 2\sigma(F^2)] = 0.058$
$wR(F^2) = 0.175$
$S = 1.11$
9475 reflections
662 parameters
0 restraints
Primary atom site location: structure-invariant direct methods
Secondary atom site location: difference Fourier map
H-atom parameters not defined
$w = 1/[\sigma^2(F_o^2) + (0.0924P)^2 + 183.152P]$ where $P = (F_o^2 + 2F_c^2)/3$
$(\Delta/\sigma)_{max} < 0.001$
$\Delta\rho_{max} = 3.11$ e Å^{-3}
$\Delta\rho_{min} = -3.90$ e Å^{-3}

Special details

Geometry. All esds (except the esd in the dihedral angle between two l.s. planes) are estimated using the full covariance matrix. The cell esds are taken into account individually in the estimation of esds in distances, angles and torsion angles; correlations between esds in cell parameters are only used when they are defined by crystal symmetry. An approximate (isotropic) treatment of cell esds is used for estimating esds involving l.s. planes.

Refinement. Oxygen atoms of the [SiO4] unit of polyoxometalate were disorderd between two positions. Tungsten, chromium, and carbon atoms refined anisotropically. Oxygen atoms of the chromium cation and polyoxometalate were refined anisotropically, while those of the disordered [SiO4] unit of polyoxometalate were refined isotropically. Oxygen atoms of the water of crystallization were refined isotropically. Nitrogen atoms of the chromium cation were refined anisotropically, while that of the ammonium ion was refined isotropically. Silicon atom of the polyoxometalate was refined isotropically. Otherwise, non-positive definite anisotropic displacement parameters were observed. Hydrogen atoms were not included in the calculation. TG and elemental analysis showed that 6 water of crystallization and 2 ammonium ion existed per formula. 3 out of the 6 water of crystallization per formula could be located.

Fractional atomic coordinates and isotropic or equivalent isotropic displacement parameters (Å²)

	x	*y*	*z*	U_{iso}*/U_{eq}	Occ. (<1)
W1	0.08250 (2)	0.22238 (2)	0.45055 (4)	0.02356 (16)	
W2	0.08301 (2)	0.36076 (2)	0.45091 (4)	0.02339 (16)	
W3	−0.00012 (2)	0.29122 (2)	0.50938 (4)	0.02474 (16)	
W4	0.08314 (2)	0.36002 (2)	0.19168 (5)	0.02883 (17)	
W5	0.0000	0.15333 (3)	0.2500	0.0382 (2)	
W6	0.0000	0.42973 (3)	0.2500	0.0330 (2)	
W7	0.08256 (2)	0.22207 (3)	0.19064 (6)	0.0415 (2)	
Cr1	0.34683 (6)	0.52309 (7)	0.52795 (15)	0.0187 (4)	
Cr2	0.24018 (6)	0.55105 (8)	0.46334 (15)	0.0209 (4)	
Cr3	0.27545 (6)	0.43017 (8)	0.52804 (16)	0.0216 (4)	
Si1	0.0000	0.29143 (15)	0.2500	0.0102 (9)*	
O1	0.0330 (5)	0.3426 (6)	0.2808 (12)	0.015 (3)*	0.5
O2	0.0294 (5)	0.2917 (6)	0.3661 (13)	0.017 (3)*	0.5
O3	0.0314 (5)	0.2395 (6)	0.2824 (12)	0.016 (3)*	0.5
O4	0.0290 (5)	0.2929 (6)	0.1733 (13)	0.016 (3)*	0.5
O5	0.0435 (4)	0.2405 (4)	0.5211 (11)	0.050 (3)	
O6	0.0432 (4)	0.3430 (4)	0.5201 (12)	0.056 (3)	
O7	0.0436 (6)	0.1669 (7)	0.3857 (13)	0.100 (7)	
O8	0.1048 (6)	0.2185 (7)	0.3406 (12)	0.097 (7)	
O9	0.1215 (3)	0.1885 (4)	0.1630 (8)	0.038 (2)	
O10	0.1046 (4)	0.2919 (4)	0.4768 (11)	0.047 (3)	
O11	0.0429 (5)	0.4156 (7)	0.3831 (9)	0.100 (7)	
O12	0.0423 (6)	0.4141 (7)	0.1891 (11)	0.096 (7)	
O13	0.1054 (4)	0.2930 (5)	0.2051 (14)	0.093 (7)	
O14	0.0000	0.4958 (5)	0.2500	0.039 (4)	
O15	0.1210 (3)	0.3943 (6)	0.1594 (8)	0.057 (4)	
O16	0.1068 (6)	0.3658 (7)	0.3421 (10)	0.092 (6)	
O17	0.0419 (5)	0.2425 (5)	0.0495 (13)	0.095 (6)	
O18	0.0000	0.0887 (5)	0.2500	0.060 (5)	
O19	0.1219 (3)	0.3939 (4)	0.5478 (9)	0.047 (3)	
O20	0.0435 (5)	0.1677 (7)	0.1940 (11)	0.098 (7)	
O21	0.1219 (4)	0.1906 (5)	0.5453 (12)	0.069 (4)	

O22	0.0437 (4)	0.3434 (4)	0.0507 (12)	0.082 (5)	
O23	0.0004 (5)	0.2928 (5)	0.6340 (10)	0.066 (4)	
O24	0.2877 (3)	0.5013 (3)	0.5074 (6)	0.0173 (17)	
O25	0.2705 (3)	0.5978 (4)	0.5828 (7)	0.033 (2)	
O26	0.3425 (3)	0.5884 (4)	0.6030 (7)	0.029 (2)	
O27	0.2634 (3)	0.5910 (3)	0.3706 (7)	0.026 (2)	
O28	0.3310 (3)	0.5608 (4)	0.3935 (6)	0.0261 (19)	
O29	0.3292 (3)	0.4201 (4)	0.6547 (7)	0.031 (2)	
O30	0.3729 (3)	0.4901 (4)	0.6696 (7)	0.029 (2)	
O31	0.3052 (3)	0.4019 (3)	0.4360 (7)	0.030 (2)	
O32	0.3597 (3)	0.4611 (3)	0.4576 (7)	0.028 (2)	
O33	0.2062 (3)	0.5206 (4)	0.5480 (7)	0.033 (2)	
O34	0.2432 (3)	0.4487 (4)	0.6222 (7)	0.032 (2)	
O35	0.2039 (3)	0.5089 (4)	0.3421 (7)	0.031 (2)	
O36	0.2193 (3)	0.4274 (4)	0.4046 (7)	0.030 (2)	
O100	−0.0246 (11)	0.3907 (14)	0.716 (3)	0.100 (11)*	0.5
O101	0.0005 (11)	0.4441 (13)	−0.053 (3)	0.091 (10)*	0.5
O102	0.0857 (12)	0.5487 (14)	0.193 (3)	0.098 (11)*	0.5
N1	0.4126 (3)	0.5440 (4)	0.5507 (8)	0.024 (2)	
N2	0.2612 (4)	0.3526 (5)	0.5604 (9)	0.031 (3)	
N3	0.1891 (4)	0.6077 (4)	0.4155 (8)	0.024 (2)	
N4	0.1116 (10)	0.5104 (11)	0.385 (2)	0.135 (10)*	
C1	0.3111 (5)	0.6074 (6)	0.6232 (10)	0.030 (3)	
C2	0.2976 (4)	0.5894 (5)	0.3479 (10)	0.023 (3)	
C3	0.3613 (4)	0.4485 (6)	0.6989 (10)	0.030 (3)	
C4	0.3386 (4)	0.4198 (5)	0.4200 (10)	0.026 (3)	
C5	0.2142 (5)	0.4830 (6)	0.6106 (11)	0.034 (3)	
C6	0.1992 (5)	0.4607 (6)	0.3377 (11)	0.032 (3)	
C7	0.4226 (4)	0.5923 (5)	0.5198 (9)	0.026 (3)	
C8	0.4656 (4)	0.6057 (5)	0.5336 (10)	0.028 (3)	
C9	0.5009 (4)	0.5710 (5)	0.5820 (11)	0.030 (3)	
C10	0.4901 (4)	0.5227 (5)	0.6123 (10)	0.026 (3)	
C11	0.4465 (5)	0.5116 (5)	0.5967 (12)	0.031 (3)	
C12	0.5477 (4)	0.5855 (6)	0.6015 (13)	0.040 (4)	
C13	0.5635 (5)	0.6284 (7)	0.6905 (14)	0.049 (4)	
C14	0.2946 (5)	0.3172 (5)	0.5903 (11)	0.030 (3)	
C15	0.2888 (4)	0.2687 (5)	0.6338 (13)	0.037 (4)	
C16	0.2480 (5)	0.2569 (6)	0.6420 (11)	0.034 (3)	
C17	0.2140 (5)	0.2925 (6)	0.6017 (13)	0.038 (4)	
C18	0.2211 (4)	0.3398 (5)	0.5617 (11)	0.030 (3)	
C19	0.2426 (7)	0.2070 (6)	0.6967 (16)	0.059 (6)	
C20	0.2542 (13)	0.2216 (15)	0.818 (3)	0.139 (13)*	
C21	0.1725 (4)	0.6287 (6)	0.4852 (12)	0.034 (3)	
C22	0.1432 (5)	0.6701 (6)	0.4588 (12)	0.041 (4)	
C23	0.1286 (5)	0.6916 (6)	0.3589 (12)	0.036 (3)	
C24	0.1449 (5)	0.6678 (6)	0.2844 (12)	0.041 (4)	
C25	0.1742 (5)	0.6273 (6)	0.3163 (10)	0.035 (3)	
C26	0.0973 (6)	0.7382 (7)	0.3252 (15)	0.054 (5)	

C27	0.1151 (12)	0.7828 (9)	0.399 (2)	0.109 (11)

Atomic displacement parameters (Å²)

	U^{11}	U^{22}	U^{33}	U^{12}	U^{13}	U^{23}
W1	0.0170 (3)	0.0282 (3)	0.0223 (3)	0.0051 (2)	0.0032 (2)	0.0032 (2)
W2	0.0180 (3)	0.0304 (3)	0.0167 (3)	0.0043 (2)	0.0000 (2)	−0.00719 (19)
W3	0.0253 (3)	0.0291 (3)	0.0165 (3)	0.0026 (2)	0.0034 (2)	0.00589 (19)
W4	0.0205 (3)	0.0255 (3)	0.0461 (4)	−0.0057 (2)	0.0187 (3)	0.0013 (2)
W5	0.0455 (5)	0.0107 (4)	0.0682 (6)	0.000	0.0323 (5)	0.000
W6	0.0635 (6)	0.0106 (4)	0.0284 (4)	0.000	0.0204 (4)	0.000
W7	0.0173 (3)	0.0444 (4)	0.0612 (5)	−0.0005 (2)	0.0121 (3)	−0.0357 (3)
Cr1	0.0154 (9)	0.0199 (10)	0.0192 (10)	0.0006 (7)	0.0042 (7)	0.0021 (7)
Cr2	0.0188 (10)	0.0258 (11)	0.0179 (10)	0.0047 (8)	0.0062 (8)	0.0005 (8)
Cr3	0.0150 (9)	0.0221 (10)	0.0273 (11)	0.0019 (8)	0.0068 (8)	0.0072 (8)
O5	0.043 (6)	0.021 (5)	0.102 (10)	−0.001 (5)	0.046 (7)	−0.007 (6)
O6	0.037 (6)	0.022 (6)	0.128 (11)	−0.001 (5)	0.051 (7)	−0.006 (6)
O7	0.106 (13)	0.132 (15)	0.097 (12)	−0.082 (12)	0.080 (11)	−0.082 (11)
O8	0.105 (12)	0.135 (14)	0.080 (10)	−0.103 (11)	0.069 (10)	−0.079 (10)
O9	0.024 (5)	0.050 (6)	0.035 (6)	0.013 (5)	0.006 (4)	−0.009 (5)
O10	0.041 (6)	0.033 (6)	0.088 (9)	0.005 (4)	0.050 (7)	−0.003 (5)
O11	0.119 (12)	0.161 (16)	0.036 (7)	0.122 (12)	0.048 (8)	0.035 (8)
O12	0.127 (13)	0.129 (14)	0.059 (8)	0.103 (12)	0.067 (9)	0.056 (9)
O13	0.038 (7)	0.047 (8)	0.122 (13)	0.008 (6)	−0.060 (8)	−0.018 (7)
O14	0.059 (10)	0.010 (6)	0.043 (9)	0.000	0.015 (7)	0.000
O15	0.031 (6)	0.107 (10)	0.032 (6)	−0.041 (6)	0.009 (5)	−0.005 (6)
O16	0.116 (13)	0.137 (14)	0.044 (8)	0.102 (11)	0.053 (8)	0.041 (8)
O17	0.067 (9)	0.029 (7)	0.125 (13)	−0.018 (6)	−0.045 (9)	−0.030 (7)
O18	0.086 (13)	0.014 (7)	0.053 (10)	0.000	−0.010 (9)	0.000
O19	0.030 (5)	0.046 (7)	0.064 (7)	−0.018 (5)	0.016 (5)	−0.043 (6)
O20	0.087 (11)	0.159 (16)	0.065 (9)	−0.101 (11)	0.047 (8)	−0.078 (10)
O21	0.037 (7)	0.063 (8)	0.105 (11)	0.027 (6)	0.022 (7)	0.071 (8)
O22	0.048 (7)	0.017 (6)	0.118 (12)	0.004 (5)	−0.047 (8)	−0.012 (6)
O23	0.108 (12)	0.057 (9)	0.056 (8)	0.036 (7)	0.058 (9)	0.021 (6)
O24	0.014 (4)	0.019 (4)	0.016 (4)	0.002 (3)	0.003 (3)	0.001 (3)
O25	0.025 (5)	0.038 (6)	0.033 (5)	0.003 (4)	0.008 (4)	−0.016 (4)
O26	0.023 (5)	0.033 (5)	0.027 (5)	−0.001 (4)	0.005 (4)	−0.007 (4)
O27	0.029 (5)	0.024 (5)	0.031 (5)	0.007 (4)	0.018 (4)	0.009 (4)
O28	0.019 (4)	0.033 (5)	0.021 (5)	0.003 (4)	0.002 (4)	0.007 (4)
O29	0.020 (5)	0.035 (5)	0.034 (5)	0.002 (4)	0.007 (4)	0.012 (4)
O30	0.022 (5)	0.040 (6)	0.020 (5)	−0.006 (4)	0.000 (4)	0.010 (4)
O31	0.031 (5)	0.016 (5)	0.043 (6)	−0.005 (4)	0.015 (4)	−0.004 (4)
O32	0.016 (4)	0.028 (5)	0.041 (5)	−0.002 (4)	0.012 (4)	−0.006 (4)
O33	0.026 (5)	0.041 (6)	0.038 (6)	0.019 (4)	0.020 (4)	0.014 (4)
O34	0.028 (5)	0.029 (5)	0.040 (6)	0.007 (4)	0.015 (4)	0.009 (4)
O35	0.029 (5)	0.028 (5)	0.031 (5)	0.008 (4)	0.007 (4)	−0.003 (4)
O36	0.025 (5)	0.021 (5)	0.041 (6)	−0.001 (4)	0.009 (4)	0.003 (4)
N1	0.022 (5)	0.020 (5)	0.029 (6)	−0.003 (4)	0.008 (5)	−0.005 (4)

N2	0.021 (6)	0.034 (7)	0.032 (6)	−0.006 (5)	0.003 (5)	−0.001 (5)
N3	0.030 (6)	0.024 (6)	0.021 (6)	0.008 (5)	0.011 (5)	−0.003 (4)
C1	0.031 (7)	0.034 (8)	0.023 (7)	0.001 (6)	0.009 (6)	−0.001 (5)
C2	0.026 (6)	0.018 (6)	0.025 (7)	0.009 (5)	0.008 (5)	0.000 (5)
C3	0.016 (6)	0.049 (9)	0.023 (7)	−0.004 (6)	0.003 (5)	0.006 (6)
C4	0.015 (6)	0.023 (7)	0.037 (8)	−0.006 (5)	0.006 (5)	0.007 (5)
C5	0.029 (7)	0.043 (9)	0.035 (8)	0.005 (7)	0.017 (6)	0.007 (7)
C6	0.032 (7)	0.036 (9)	0.028 (7)	0.002 (6)	0.009 (6)	−0.009 (6)
C7	0.022 (6)	0.036 (8)	0.014 (6)	−0.004 (5)	−0.003 (5)	0.005 (5)
C8	0.023 (6)	0.031 (7)	0.028 (7)	0.001 (6)	0.009 (5)	0.006 (6)
C9	0.014 (6)	0.031 (7)	0.041 (8)	−0.006 (5)	0.007 (5)	0.003 (6)
C10	0.017 (6)	0.028 (7)	0.032 (7)	0.001 (5)	0.006 (5)	0.004 (5)
C11	0.034 (8)	0.018 (7)	0.044 (9)	0.005 (6)	0.016 (6)	−0.001 (6)
C12	0.015 (6)	0.036 (8)	0.066 (11)	−0.005 (6)	0.011 (7)	0.006 (7)
C13	0.038 (9)	0.054 (11)	0.053 (10)	−0.016 (8)	0.011 (8)	−0.013 (8)
C14	0.029 (7)	0.024 (7)	0.033 (8)	0.007 (6)	0.006 (6)	0.008 (6)
C15	0.021 (7)	0.018 (7)	0.061 (10)	−0.006 (5)	0.000 (6)	0.005 (6)
C16	0.029 (7)	0.033 (8)	0.037 (8)	−0.016 (6)	0.010 (6)	0.012 (6)
C17	0.020 (7)	0.044 (10)	0.049 (10)	−0.005 (6)	0.011 (7)	0.017 (7)
C18	0.022 (7)	0.029 (7)	0.038 (8)	−0.014 (6)	0.009 (6)	−0.002 (6)
C19	0.062 (12)	0.035 (10)	0.064 (12)	−0.025 (8)	0.003 (10)	0.020 (8)
C21	0.023 (7)	0.037 (8)	0.041 (8)	0.010 (6)	0.009 (6)	−0.005 (6)
C22	0.046 (9)	0.035 (8)	0.046 (9)	0.018 (7)	0.022 (7)	−0.007 (7)
C23	0.027 (7)	0.034 (8)	0.050 (10)	0.008 (6)	0.016 (7)	0.008 (7)
C24	0.039 (9)	0.046 (9)	0.032 (8)	0.004 (7)	0.007 (7)	−0.001 (7)
C25	0.035 (8)	0.040 (8)	0.017 (7)	0.016 (6)	−0.007 (6)	−0.004 (6)
C26	0.038 (9)	0.040 (10)	0.084 (13)	0.022 (8)	0.022 (9)	0.001 (9)
C27	0.17 (3)	0.048 (13)	0.080 (18)	0.018 (16)	0.013 (19)	−0.011 (12)

Geometric parameters (Å, º)

W1—O21	1.663 (10)	Cr2—N3	2.116 (10)
W1—O8	1.875 (13)	Cr3—O24	1.901 (8)
W1—O7	1.891 (13)	Cr3—O31	1.964 (9)
W1—O5	1.891 (10)	Cr3—O34	1.973 (9)
W1—O10	1.900 (10)	Cr3—O29	1.975 (9)
W1—O3	2.331 (15)	Cr3—O36	1.983 (9)
W1—O2	2.447 (15)	Cr3—N2	2.114 (12)
W2—O19	1.687 (9)	Si1—O2	1.521 (16)
W2—O10	1.878 (10)	Si1—O2^{i}	1.521 (16)
W2—O16	1.896 (12)	Si1—O4^{i}	1.630 (16)
W2—O6	1.898 (11)	Si1—O4	1.630 (16)
W2—O11	1.908 (12)	Si1—O3^{i}	1.633 (15)
W2—O1	2.342 (15)	Si1—O3	1.633 (15)
W2—O2	2.454 (15)	Si1—O1^{i}	1.645 (15)
W3—O23	1.685 (12)	Si1—O1	1.645 (15)
W3—O17^{i}	1.799 (14)	O1—O2	1.77 (2)
W3—O5	1.879 (10)	O2—O4^{i}	1.77 (2)

W3—O6	1.893 (10)	O2—O3	1.77 (2)
W3—O22^{i}	1.899 (11)	O4—O2^{i}	1.77 (2)
W3—O4^{i}	2.315 (16)	O4—W3^{i}	2.315 (16)
W3—O2	2.450 (16)	O17—W3^{i}	1.800 (14)
W4—O15	1.685 (10)	O22—W3^{i}	1.898 (11)
W4—O13	1.841 (12)	O25—C1	1.250 (16)
W4—O12	1.903 (12)	O26—C1	1.241 (16)
W4—O16	1.911 (13)	O27—C2	1.251 (15)
W4—O22	1.929 (12)	O28—C2	1.266 (14)
W4—O1	2.383 (15)	O29—C3	1.233 (16)
W4—O4	2.398 (15)	O30—C3	1.239 (16)
W5—O18	1.652 (14)	O31—C4	1.258 (15)
W5—O20^{i}	1.856 (13)	O32—C4	1.263 (15)
W5—O20	1.856 (13)	O33—C5	1.246 (17)
W5—O7^{i}	1.908 (16)	O34—C5	1.250 (17)
W5—O7	1.908 (16)	O35—C6	1.239 (17)
W5—O3	2.397 (15)	O36—C6	1.243 (17)
W5—O3^{i}	2.397 (15)	O100—O100^{ii}	1.53 (7)
W6—O14	1.687 (12)	N1—C11	1.336 (17)
W6—O12	1.874 (12)	N1—C7	1.378 (16)
W6—O12^{i}	1.874 (12)	N2—C18	1.345 (17)
W6—O11^{i}	1.877 (13)	N2—C14	1.352 (17)
W6—O11	1.877 (13)	N3—C21	1.351 (17)
W6—O1	2.438 (15)	N3—C25	1.353 (17)
W6—O1^{i}	2.438 (15)	C7—C8	1.375 (18)
W7—O9	1.671 (9)	C8—C9	1.411 (18)
W7—O20	1.889 (13)	C9—C10	1.382 (18)
W7—O8	1.902 (16)	C9—C12	1.485 (17)
W7—O13	1.938 (13)	C10—C11	1.379 (18)
W7—O17	1.967 (14)	C12—C13	1.57 (2)
W7—O3	2.438 (15)	C14—C15	1.41 (2)
W7—O4	2.456 (15)	C15—C16	1.396 (19)
Cr1—O24	1.913 (8)	C16—C17	1.38 (2)
Cr1—O28	1.963 (8)	C16—C19	1.516 (19)
Cr1—O32	1.968 (9)	C17—C18	1.376 (19)
Cr1—O26	1.985 (9)	C19—C20	1.59 (4)
Cr1—O30	1.989 (8)	C21—C22	1.378 (19)
Cr1—N1	2.105 (10)	C22—C23	1.38 (2)
Cr2—O24	1.917 (8)	C23—C24	1.43 (2)
Cr2—O27	1.964 (8)	C23—C26	1.52 (2)
Cr2—O35	1.966 (9)	C24—C25	1.36 (2)
Cr2—O25	1.970 (9)	C26—C27	1.49 (3)
Cr2—O33	2.008 (9)		

O21—W1—O8	100.6 (8)	O27—Cr2—O33	168.3 (4)
O21—W1—O7	101.1 (8)	O35—Cr2—O33	88.9 (4)
O8—W1—O7	88.3 (5)	O25—Cr2—O33	88.8 (4)
O21—W1—O5	101.2 (6)	O24—Cr2—N3	178.4 (4)

O8—W1—O5	158.3 (8)	O27—Cr2—N3	83.3 (4)
O7—W1—O5	88.1 (5)	O35—Cr2—N3	87.2 (4)
O21—W1—O10	100.3 (7)	O25—Cr2—N3	86.7 (4)
O8—W1—O10	88.4 (5)	O33—Cr2—N3	85.1 (4)
O7—W1—O10	158.6 (8)	O24—Cr3—O31	94.8 (4)
O5—W1—O10	87.1 (4)	O24—Cr3—O34	92.9 (4)
O21—W1—O3	158.1 (7)	O31—Cr3—O34	172.2 (4)
O8—W1—O3	64.5 (7)	O24—Cr3—O29	95.0 (4)
O7—W1—O3	64.1 (7)	O31—Cr3—O29	91.5 (4)
O5—W1—O3	94.7 (5)	O34—Cr3—O29	88.4 (4)
O10—W1—O3	95.5 (6)	O24—Cr3—O36	94.9 (4)
O21—W1—O2	158.6 (7)	O31—Cr3—O36	87.6 (4)
O8—W1—O2	94.0 (8)	O34—Cr3—O36	91.1 (4)
O7—W1—O2	94.9 (8)	O29—Cr3—O36	170.1 (4)
O5—W1—O2	65.0 (5)	O24—Cr3—N2	176.2 (4)
O10—W1—O2	64.2 (5)	O31—Cr3—N2	88.8 (4)
O3—W1—O2	43.3 (5)	O34—Cr3—N2	83.5 (4)
O19—W2—O10	101.6 (6)	O29—Cr3—N2	83.5 (4)
O19—W2—O16	100.1 (7)	O36—Cr3—N2	86.6 (4)
O10—W2—O16	89.0 (5)	O2—Si1—O2^{i}	179.6 (12)
O19—W2—O6	100.5 (6)	O2—Si1—O4^{i}	68.1 (8)
O10—W2—O6	87.5 (4)	O2^{i}—Si1—O4^{i}	111.9 (8)
O16—W2—O6	159.3 (7)	O2—Si1—O4	111.9 (8)
O19—W2—O11	101.3 (7)	O2^{i}—Si1—O4	68.1 (8)
O10—W2—O11	157.1 (7)	O4^{i}—Si1—O4	177.4 (10)
O16—W2—O11	88.3 (5)	O2—Si1—O3^{i}	112.3 (8)
O6—W2—O11	87.1 (6)	O2^{i}—Si1—O3^{i}	68.0 (8)
O19—W2—O1	157.9 (6)	O4^{i}—Si1—O3^{i}	75.4 (7)
O10—W2—O1	94.5 (6)	O4—Si1—O3^{i}	106.8 (8)
O16—W2—O1	64.9 (7)	O2—Si1—O3	68.0 (8)
O6—W2—O1	95.1 (6)	O2^{i}—Si1—O3	112.3 (8)
O11—W2—O1	63.8 (6)	O4^{i}—Si1—O3	106.8 (8)
O19—W2—O2	158.7 (6)	O4—Si1—O3	75.3 (7)
O10—W2—O2	64.3 (5)	O3^{i}—Si1—O3	71.2 (11)
O16—W2—O2	95.7 (7)	O2—Si1—O1^{i}	111.6 (8)
O6—W2—O2	64.5 (5)	O2^{i}—Si1—O1^{i}	68.0 (8)
O11—W2—O2	93.3 (7)	O4^{i}—Si1—O1^{i}	71.1 (7)
O1—W2—O2	43.3 (5)	O4—Si1—O1^{i}	106.7 (8)
O23—W3—O17^{i}	101.5 (8)	O3^{i}—Si1—O1^{i}	107.1 (8)
O23—W3—O5	101.1 (6)	O3—Si1—O1^{i}	177.7 (7)
O17^{i}—W3—O5	89.0 (6)	O2—Si1—O1	68.0 (8)
O23—W3—O6	99.4 (7)	O2^{i}—Si1—O1	111.6 (8)
O17^{i}—W3—O6	159.1 (8)	O4^{i}—Si1—O1	106.7 (8)
O5—W3—O6	87.9 (5)	O4—Si1—O1	71.1 (7)
O23—W3—O22^{i}	98.9 (7)	O3^{i}—Si1—O1	177.7 (7)
O17^{i}—W3—O22^{i}	88.3 (5)	O3—Si1—O1	107.1 (8)
O5—W3—O22^{i}	160.0 (7)	O1^{i}—Si1—O1	74.6 (11)
O6—W3—O22^{i}	87.5 (5)	Si1—O1—O2	52.7 (7)

O23—W3—O4^{i}	158.3 (7)	Si1—O1—W2	124.4 (8)
O17^{i}—W3—O4^{i}	65.5 (7)	O2—O1—W2	71.7 (7)
O5—W3—O4^{i}	96.2 (6)	Si1—O1—W4	121.0 (8)
O6—W3—O4^{i}	94.2 (6)	O2—O1—W4	133.1 (9)
O22^{i}—W3—O4^{i}	64.8 (6)	W2—O1—W4	96.2 (5)
O23—W3—O2	158.1 (7)	Si1—O1—W6	118.6 (8)
O17^{i}—W3—O2	95.4 (7)	O2—O1—W6	131.0 (9)
O5—W3—O2	65.1 (5)	W2—O1—W6	95.4 (5)
O6—W3—O2	64.7 (5)	W4—O1—W6	94.5 (5)
O22^{i}—W3—O2	95.4 (7)	Si1—O2—O4^{i}	58.8 (8)
O4^{i}—W3—O2	43.4 (5)	Si1—O2—O3	59.0 (7)
O15—W4—O13	102.4 (8)	O4^{i}—O2—O3	95.7 (10)
O15—W4—O12	100.4 (7)	Si1—O2—O1	59.3 (7)
O13—W4—O12	157.1 (8)	O4^{i}—O2—O1	95.8 (10)
O15—W4—O16	100.7 (7)	O3—O2—O1	96.3 (11)
O13—W4—O16	88.4 (7)	Si1—O2—W1	123.8 (8)
O12—W4—O16	88.6 (6)	O4^{i}—O2—W1	130.5 (9)
O15—W4—O22	98.1 (6)	O3—O2—W1	64.8 (7)
O13—W4—O22	89.4 (5)	O1—O2—W1	129.6 (10)
O12—W4—O22	86.1 (6)	Si1—O2—W3	123.1 (9)
O16—W4—O22	161.1 (8)	O4^{i}—O2—W3	64.2 (7)
O15—W4—O1	156.5 (6)	O3—O2—W3	128.3 (9)
O13—W4—O1	95.0 (8)	O1—O2—W3	130.9 (9)
O12—W4—O1	63.4 (6)	W1—O2—W3	91.8 (5)
O16—W4—O1	63.8 (6)	Si1—O2—W2	124.3 (8)
O22—W4—O1	97.7 (6)	O4^{i}—O2—W2	128.9 (9)
O15—W4—O4	156.2 (6)	O3—O2—W2	131.5 (10)
O13—W4—O4	65.7 (6)	O1—O2—W2	65.0 (7)
O12—W4—O4	92.4 (7)	W1—O2—W2	92.3 (6)
O16—W4—O4	99.5 (7)	W3—O2—W2	92.3 (5)
O22—W4—O4	62.6 (6)	Si1—O3—O2	53.0 (7)
O1—W4—O4	46.9 (5)	Si1—O3—W1	124.8 (8)
O18—W5—O20^{i}	101.4 (6)	O2—O3—W1	71.8 (7)
O18—W5—O20	101.4 (6)	Si1—O3—W5	121.0 (8)
O20^{i}—W5—O20	157.3 (12)	O2—O3—W5	134.4 (9)
O18—W5—O7^{i}	100.4 (6)	W1—O3—W5	96.5 (6)
O20^{i}—W5—O7^{i}	87.3 (6)	Si1—O3—W7	118.7 (8)
O20—W5—O7^{i}	88.6 (7)	O2—O3—W7	130.7 (9)
O18—W5—O7	100.4 (6)	W1—O3—W7	95.3 (5)
O20^{i}—W5—O7	88.6 (7)	W5—O3—W7	93.4 (5)
O20—W5—O7	87.3 (6)	Si1—O4—O2^{i}	53.0 (7)
O7^{i}—W5—O7	159.1 (12)	Si1—O4—W3^{i}	125.3 (9)
O18—W5—O3	156.6 (4)	O2^{i}—O4—W3^{i}	72.4 (7)
O20^{i}—W5—O3	94.4 (7)	Si1—O4—W4	120.9 (8)
O20—W5—O3	64.0 (6)	O2^{i}—O4—W4	134.7 (9)
O7^{i}—W5—O3	97.4 (7)	W3^{i}—O4—W4	97.2 (6)
O7—W5—O3	62.5 (7)	Si1—O4—W7	117.9 (8)
O18—W5—O3^{i}	156.6 (4)	O2^{i}—O4—W7	130.9 (9)

O20^{i}—W5—O3^{i}	64.0 (6)	W3^{i}—O4—W7	95.2 (5)
O20—W5—O3^{i}	94.4 (7)	W4—O4—W7	93.1 (6)
O7^{i}—W5—O3^{i}	62.5 (7)	W3—O5—W1	137.8 (7)
O7—W5—O3^{i}	97.4 (7)	W3—O6—W2	137.9 (7)
O3—W5—O3^{i}	46.7 (7)	W1—O7—W5	136.4 (11)
O14—W6—O12	102.3 (5)	W1—O8—W7	138.0 (11)
O14—W6—O12^{i}	102.3 (5)	W2—O10—W1	138.7 (7)
O12—W6—O12^{i}	155.5 (11)	W6—O11—W2	138.3 (9)
O14—W6—O11^{i}	101.1 (6)	W6—O12—W4	139.1 (8)
O12—W6—O11^{i}	86.5 (7)	W4—O13—W7	137.6 (8)
O12^{i}—W6—O11^{i}	88.8 (6)	W2—O16—W4	134.9 (10)
O14—W6—O11	101.1 (6)	W3^{i}—O17—W7	138.6 (9)
O12—W6—O11	88.8 (6)	W5—O20—W7	139.9 (9)
O12^{i}—W6—O11	86.5 (7)	W3^{i}—O22—W4	135.0 (9)
O11^{i}—W6—O11	157.8 (12)	Cr3—O24—Cr1	120.4 (4)
O14—W6—O1	155.9 (4)	Cr3—O24—Cr2	119.6 (4)
O12—W6—O1	62.5 (6)	Cr1—O24—Cr2	120.0 (4)
O12^{i}—W6—O1	94.2 (7)	C1—O25—Cr2	128.0 (9)
O11^{i}—W6—O1	96.7 (7)	C1—O26—Cr1	130.8 (9)
O11—W6—O1	62.1 (6)	C2—O27—Cr2	135.5 (8)
O14—W6—O1^{i}	155.9 (4)	C2—O28—Cr1	129.1 (8)
O12—W6—O1^{i}	94.2 (7)	C3—O29—Cr3	132.3 (9)
O12^{i}—W6—O1^{i}	62.5 (6)	C3—O30—Cr1	126.9 (8)
O11^{i}—W6—O1^{i}	62.1 (6)	C4—O31—Cr3	128.3 (9)
O11—W6—O1^{i}	96.7 (7)	C4—O32—Cr1	133.7 (8)
O1—W6—O1^{i}	48.3 (7)	C5—O33—Cr2	131.7 (9)
O9—W7—O20	101.0 (7)	C5—O34—Cr3	129.2 (9)
O9—W7—O8	100.9 (7)	C6—O35—Cr2	127.6 (9)
O20—W7—O8	86.5 (6)	C6—O36—Cr3	132.4 (9)
O9—W7—O13	102.3 (7)	C11—N1—C7	117.1 (11)
O20—W7—O13	156.6 (8)	C11—N1—Cr1	121.8 (9)
O8—W7—O13	87.2 (7)	C7—N1—Cr1	121.1 (8)
O9—W7—O17	102.3 (6)	C18—N2—C14	120.1 (12)
O20—W7—O17	89.9 (7)	C18—N2—Cr3	120.9 (10)
O8—W7—O17	156.8 (8)	C14—N2—Cr3	118.7 (9)
O13—W7—O17	87.0 (5)	C21—N3—C25	117.4 (11)
O9—W7—O3	155.4 (5)	C21—N3—Cr2	121.2 (9)
O20—W7—O3	62.7 (6)	C25—N3—Cr2	121.3 (8)
O8—W7—O3	61.9 (6)	O26—C1—O25	129.7 (13)
O13—W7—O3	94.6 (7)	O27—C2—O28	124.9 (12)
O17—W7—O3	96.3 (7)	O29—C3—O30	130.3 (12)
O9—W7—O4	156.5 (5)	O31—C4—O32	127.4 (13)
O20—W7—O4	95.2 (7)	O33—C5—O34	126.1 (13)
O8—W7—O4	97.0 (7)	O35—C6—O36	128.4 (13)
O13—W7—O4	63.3 (6)	C8—C7—N1	121.1 (12)
O17—W7—O4	60.5 (6)	C7—C8—C9	121.1 (12)
O3—W7—O4	48.1 (5)	C10—C9—C8	116.8 (11)
O24—Cr1—O28	95.3 (3)	C10—C9—C12	121.2 (12)

O24—Cr1—O32	93.9 (3)	C8—C9—C12	122.0 (12)
O28—Cr1—O32	88.5 (4)	C11—C10—C9	119.5 (12)
O24—Cr1—O26	94.1 (4)	N1—C11—C10	124.4 (13)
O28—Cr1—O26	91.2 (4)	C9—C12—C13	109.9 (13)
O32—Cr1—O26	172.0 (4)	N2—C14—C15	120.2 (13)
O24—Cr1—O30	94.3 (4)	C16—C15—C14	119.3 (13)
O28—Cr1—O30	170.3 (4)	C17—C16—C15	117.9 (12)
O32—Cr1—O30	92.1 (4)	C17—C16—C19	122.4 (14)
O26—Cr1—O30	86.8 (4)	C15—C16—C19	119.7 (15)
O24—Cr1—N1	177.8 (4)	C18—C17—C16	121.1 (13)
O28—Cr1—N1	85.8 (4)	N2—C18—C17	121.0 (13)
O32—Cr1—N1	84.1 (4)	C16—C19—C20	106.4 (19)
O26—Cr1—N1	87.9 (4)	N3—C21—C22	122.0 (13)
O30—Cr1—N1	84.7 (4)	C21—C22—C23	121.6 (14)
O24—Cr2—O27	95.7 (4)	C22—C23—C24	116.0 (13)
O24—Cr2—O35	94.0 (4)	C22—C23—C26	124.4 (14)
O27—Cr2—O35	90.0 (4)	C24—C23—C26	119.6 (14)
O24—Cr2—O25	92.1 (4)	C25—C24—C23	119.2 (14)
O27—Cr2—O25	91.1 (4)	N3—C25—C24	123.7 (13)
O35—Cr2—O25	173.6 (4)	C27—C26—C23	109.9 (17)
O24—Cr2—O33	96.0 (3)		

O2^{i}—Si1—O1—O2	179.8 (6)	O1—Si1—O4—W4	1.3 (8)
O4^{i}—Si1—O1—O2	57.3 (9)	O2—Si1—O4—W7	58.5 (10)
O4—Si1—O1—O2	−124.2 (9)	O2^{i}—Si1—O4—W7	−122.0 (10)
O3—Si1—O1—O2	−56.9 (9)	O3^{i}—Si1—O4—W7	−64.8 (10)
O1^{i}—Si1—O1—O2	121.6 (10)	O3—Si1—O4—W7	−0.1 (8)
O2—Si1—O1—W2	−1.4 (9)	O1^{i}—Si1—O4—W7	−179.1 (8)
O2^{i}—Si1—O1—W2	178.4 (9)	O1—Si1—O4—W7	114.2 (10)
O4^{i}—Si1—O1—W2	55.9 (11)	O23—W3—O5—W1	−155.7 (10)
O4—Si1—O1—W2	−125.6 (11)	O17^{i}—W3—O5—W1	102.8 (11)
O3—Si1—O1—W2	−58.3 (11)	O6—W3—O5—W1	−56.5 (10)
O1^{i}—Si1—O1—W2	120.2 (13)	O22^{i}—W3—O5—W1	20 (2)
O2—Si1—O1—W4	122.9 (11)	O4^{i}—W3—O5—W1	37.5 (10)
O2^{i}—Si1—O1—W4	−57.3 (11)	O2—W3—O5—W1	6.4 (9)
O4^{i}—Si1—O1—W4	−179.8 (8)	O21—W1—O5—W3	156.3 (10)
O4—Si1—O1—W4	−1.3 (8)	O8—W1—O5—W3	−22 (2)
O3—Si1—O1—W4	66.0 (10)	O7—W1—O5—W3	−102.7 (11)
O1^{i}—Si1—O1—W4	−115.5 (12)	O10—W1—O5—W3	56.4 (10)
O2—Si1—O1—W6	−121.6 (10)	O3—W1—O5—W3	−38.9 (10)
O2^{i}—Si1—O1—W6	58.2 (10)	O2—W1—O5—W3	−6.4 (9)
O4^{i}—Si1—O1—W6	−64.3 (10)	O23—W3—O6—W2	155.6 (10)
O4—Si1—O1—W6	114.2 (10)	O17^{i}—W3—O6—W2	−27 (2)
O3—Si1—O1—W6	−178.5 (7)	O5—W3—O6—W2	54.8 (11)
O1^{i}—Si1—O1—W6	0.000 (1)	O22^{i}—W3—O6—W2	−105.7 (11)
O4—Si1—O2—O4^{i}	177.2 (11)	O4^{i}—W3—O6—W2	−41.3 (11)
O3^{i}—Si1—O2—O4^{i}	−62.7 (9)	O2—W3—O6—W2	−8.5 (9)
O3—Si1—O2—O4^{i}	−119.9 (9)	O19—W2—O6—W3	−155.5 (10)

O1^{i}—Si1—O2—O4^{i}	57.7 (9)	O10—W2—O6—W3	−54.1 (11)
O1—Si1—O2—O4^{i}	119.8 (9)	O16—W2—O6—W3	26 (2)
O4^{i}—Si1—O2—O3	119.9 (9)	O11—W2—O6—W3	103.6 (11)
O4—Si1—O2—O3	−62.9 (9)	O1—W2—O6—W3	40.2 (11)
O3^{i}—Si1—O2—O3	57.2 (12)	O2—W2—O6—W3	8.5 (9)
O1^{i}—Si1—O2—O3	177.6 (8)	O21—W1—O7—W5	−155.5 (12)
O1—Si1—O2—O3	−120.3 (10)	O8—W1—O7—W5	−55.1 (13)
O4^{i}—Si1—O2—O1	−119.8 (9)	O5—W1—O7—W5	103.5 (12)
O4—Si1—O2—O1	57.4 (9)	O10—W1—O7—W5	26 (2)
O3^{i}—Si1—O2—O1	177.6 (8)	O3—W1—O7—W5	7.3 (10)
O3—Si1—O2—O1	120.3 (10)	O2—W1—O7—W5	38.8 (12)
O1^{i}—Si1—O2—O1	−62.1 (12)	O21—W1—O8—W7	157.0 (13)
O4^{i}—Si1—O2—W1	120.5 (11)	O7—W1—O8—W7	56.0 (14)
O4—Si1—O2—W1	−62.3 (11)	O5—W1—O8—W7	−25 (2)
O3^{i}—Si1—O2—W1	57.9 (12)	O10—W1—O8—W7	−102.9 (13)
O3—Si1—O2—W1	0.6 (8)	O3—W1—O8—W7	−6.0 (11)
O1^{i}—Si1—O2—W1	178.2 (8)	O2—W1—O8—W7	−38.8 (13)
O1—Si1—O2—W1	−119.7 (12)	O19—W2—O10—W1	155.8 (10)
O4^{i}—Si1—O2—W3	1.8 (8)	O16—W2—O10—W1	−104.1 (11)
O4—Si1—O2—W3	179.0 (8)	O6—W2—O10—W1	55.6 (10)
O3^{i}—Si1—O2—W3	−60.9 (11)	O11—W2—O10—W1	−20.9 (19)
O3—Si1—O2—W3	−118.1 (11)	O1—W2—O10—W1	−39.3 (10)
O1^{i}—Si1—O2—W3	59.5 (11)	O2—W2—O10—W1	−7.3 (9)
O1—Si1—O2—W3	121.5 (11)	O21—W1—O10—W2	−157.1 (10)
O4^{i}—Si1—O2—W2	−118.4 (11)	O8—W1—O10—W2	102.5 (12)
O4—Si1—O2—W2	58.8 (12)	O7—W1—O10—W2	21 (2)
O3^{i}—Si1—O2—W2	178.9 (8)	O5—W1—O10—W2	−56.2 (10)
O3—Si1—O2—W2	121.7 (12)	O3—W1—O10—W2	38.3 (10)
O1^{i}—Si1—O2—W2	−60.7 (12)	O2—W1—O10—W2	7.3 (9)
O1—Si1—O2—W2	1.3 (8)	O14—W6—O11—W2	−154.8 (13)
W2—O1—O2—Si1	178.8 (8)	O12—W6—O11—W2	−52.5 (15)
W4—O1—O2—Si1	−100.1 (12)	O12^{i}—W6—O11—W2	103.4 (15)
W6—O1—O2—Si1	97.7 (11)	O11^{i}—W6—O11—W2	25.2 (13)
Si1—O1—O2—O4^{i}	−48.3 (7)	O1—W6—O11—W2	6.8 (12)
W2—O1—O2—O4^{i}	130.5 (8)	O1^{i}—W6—O11—W2	41.6 (15)
W4—O1—O2—O4^{i}	−148.4 (11)	O14—W6—O12—W4	152.2 (15)
W6—O1—O2—O4^{i}	49.4 (14)	O12^{i}—W6—O12—W4	−27.8 (15)
Si1—O1—O2—O3	48.1 (8)	O11^{i}—W6—O12—W4	−107.2 (17)
W2—O1—O2—O3	−133.1 (9)	O11—W6—O12—W4	51.1 (17)
W4—O1—O2—O3	−52.0 (15)	O1—W6—O12—W4	−7.8 (13)
W6—O1—O2—O3	145.8 (10)	O1^{i}—W6—O12—W4	−45.6 (17)
Si1—O1—O2—W1	110.4 (12)	O15—W4—O13—W7	−152.7 (15)
W2—O1—O2—W1	−70.8 (10)	O12—W4—O13—W7	24 (3)
W4—O1—O2—W1	10.3 (19)	O16—W4—O13—W7	106.7 (17)
W6—O1—O2—W1	−151.9 (8)	O22—W4—O13—W7	−54.5 (17)
Si1—O1—O2—W3	−109.0 (12)	O1—W4—O13—W7	43.1 (16)
W2—O1—O2—W3	69.8 (11)	O4—W4—O13—W7	5.5 (14)
W4—O1—O2—W3	151.0 (9)	O19—W2—O16—W4	−158.6 (11)

W6—O1—O2—W3	−11.2 (19)	O10—W2—O16—W4	99.8 (12)
Si1—O1—O2—W2	−178.8 (8)	O6—W2—O16—W4	20 (2)
W4—O1—O2—W2	81.2 (11)	O11—W2—O16—W4	−57.5 (13)
W6—O1—O2—W2	−81.1 (10)	O1—W2—O16—W4	4.3 (10)
O2^{i}—Si1—O3—O2	179.8 (6)	O2—W2—O16—W4	35.7 (12)
O4^{i}—Si1—O3—O2	−57.2 (9)	O18—W5—O20—W7	−157.9 (15)
O4—Si1—O3—O2	121.3 (9)	O20^{i}—W5—O20—W7	22.1 (15)
O3^{i}—Si1—O3—O2	−124.7 (11)	O7^{i}—W5—O20—W7	101.8 (17)
O1—Si1—O3—O2	56.9 (9)	O7—W5—O20—W7	−57.7 (17)
O2—Si1—O3—W1	−0.7 (9)	O3—W5—O20—W7	2.8 (14)
O2^{i}—Si1—O3—W1	179.1 (9)	O3^{i}—W5—O20—W7	39.5 (17)
O4^{i}—Si1—O3—W1	−57.9 (11)	O9—W7—O20—W5	157.6 (15)
O4—Si1—O3—W1	120.7 (11)	O8—W7—O20—W5	57.2 (17)
O3^{i}—Si1—O3—W1	−125.4 (14)	O13—W7—O20—W5	−18 (3)
O1—Si1—O3—W1	56.2 (11)	O17—W7—O20—W5	−99.9 (17)
O2—Si1—O3—W5	124.7 (11)	O3—W7—O20—W5	−2.8 (13)
O2^{i}—Si1—O3—W5	−55.5 (11)	O4—W7—O20—W5	−39.5 (17)
O4^{i}—Si1—O3—W5	67.5 (10)	Cr1—O26—C1—O25	−18 (2)
O4—Si1—O3—W5	−113.9 (10)	Cr2—O25—C1—O26	−4 (2)
O3^{i}—Si1—O3—W5	−0.001 (1)	Cr2—O27—C2—O28	−8 (2)
O1—Si1—O3—W5	−178.4 (7)	Cr1—O28—C2—O27	−14.9 (19)
O2—Si1—O3—W7	−121.3 (11)	Cr3—O29—C3—O30	−11 (2)
O2^{i}—Si1—O3—W7	58.5 (11)	Cr1—O30—C3—O29	−8 (2)
O4^{i}—Si1—O3—W7	−178.5 (8)	Cr3—O31—C4—O32	−2 (2)
O4—Si1—O3—W7	0.1 (8)	Cr1—O32—C4—O31	−15 (2)
O3^{i}—Si1—O3—W7	114.0 (12)	Cr2—O33—C5—O34	−13 (2)
O1—Si1—O3—W7	−64.4 (10)	Cr3—O34—C5—O33	−17 (2)
O4^{i}—O2—O3—Si1	48.2 (7)	Cr2—O35—C6—O36	−7 (2)
O1—O2—O3—Si1	−48.3 (8)	Cr3—O36—C6—O35	−17 (2)
W1—O2—O3—Si1	−179.4 (8)	C11—N1—C7—C8	1.5 (19)
W3—O2—O3—Si1	109.6 (12)	Cr1—N1—C7—C8	−179.3 (10)
W2—O2—O3—Si1	−110.2 (12)	N1—C7—C8—C9	−1 (2)
Si1—O2—O3—W1	179.4 (8)	C7—C8—C9—C10	1 (2)
O4^{i}—O2—O3—W1	−132.4 (8)	C7—C8—C9—C12	−177.6 (14)
O1—O2—O3—W1	131.1 (9)	C8—C9—C10—C11	−2 (2)
W3—O2—O3—W1	−70.9 (10)	C12—C9—C10—C11	177.4 (14)
W2—O2—O3—W1	69.2 (11)	C7—N1—C11—C10	−2 (2)
Si1—O2—O3—W5	−99.5 (12)	Cr1—N1—C11—C10	179.0 (11)
O4^{i}—O2—O3—W5	−51.3 (15)	C9—C10—C11—N1	2 (2)
O1—O2—O3—W5	−147.8 (11)	C10—C9—C12—C13	−109.1 (16)
W1—O2—O3—W5	81.1 (11)	C8—C9—C12—C13	69.8 (18)
W3—O2—O3—W5	10 (2)	C18—N2—C14—C15	−7 (2)
W2—O2—O3—W5	150.3 (9)	Cr3—N2—C14—C15	166.6 (11)
Si1—O2—O3—W7	98.3 (11)	N2—C14—C15—C16	2 (2)
O4^{i}—O2—O3—W7	146.5 (10)	C14—C15—C16—C17	3 (2)
O1—O2—O3—W7	50.0 (14)	C14—C15—C16—C19	−175.0 (15)
W1—O2—O3—W7	−81.2 (10)	C15—C16—C17—C18	−5 (2)
W3—O2—O3—W7	−152.1 (8)	C19—C16—C17—C18	173.6 (16)

W2—O2—O3—W7	−12.0 (19)	C14—N2—C18—C17	6 (2)
O2—Si1—O4—O2^{i}	−179.5 (12)	Cr3—N2—C18—C17	−167.7 (12)
O3^{i}—Si1—O4—O2^{i}	57.1 (9)	C16—C17—C18—N2	0 (2)
O3—Si1—O4—O2^{i}	121.9 (9)	C17—C16—C19—C20	−87 (2)
O1^{i}—Si1—O4—O2^{i}	−57.2 (9)	C15—C16—C19—C20	91 (2)
O1—Si1—O4—O2^{i}	−123.9 (9)	C25—N3—C21—C22	−3 (2)
O2—Si1—O4—W3^{i}	178.5 (8)	Cr2—N3—C21—C22	171.9 (12)
O2^{i}—Si1—O4—W3^{i}	−1.9 (9)	N3—C21—C22—C23	1 (2)
O3^{i}—Si1—O4—W3^{i}	55.2 (11)	C21—C22—C23—C24	1 (2)
O3—Si1—O4—W3^{i}	120.0 (10)	C21—C22—C23—C26	−178.2 (16)
O1^{i}—Si1—O4—W3^{i}	−59.1 (11)	C22—C23—C24—C25	−2 (2)
O1—Si1—O4—W3^{i}	−125.8 (11)	C26—C23—C24—C25	177.6 (15)
O2—Si1—O4—W4	−54.4 (11)	C21—N3—C25—C24	2 (2)
O2^{i}—Si1—O4—W4	125.2 (11)	Cr2—N3—C25—C24	−172.6 (12)
O3^{i}—Si1—O4—W4	−177.7 (8)	C23—C24—C25—N3	0 (2)
O3—Si1—O4—W4	−112.9 (10)	C22—C23—C26—C27	53 (3)
O1^{i}—Si1—O4—W4	68.0 (10)	C24—C23—C26—C27	−126 (2)

Symmetry codes: (i) −*x*, *y*, −*z*+1/2; (ii) −*x*, *y*, −*z*+3/2.